AIP | Applied Physics Letters

Optical gain analysis of c-InGaN quantum wells on unstrained c-In0.31Ga0.69N templates

Teruhisa Kotani, Paolo Lugli, and Chihiro Hamaguchi

Citation: Appl. Phys. Lett. **102**, 011128 (2013); doi: 10.1063/1.4774290
View online: http://dx.doi.org/10.1063/1.4774290
View Table of Contents: http://apl.aip.org/resource/1/APPLAB/v102/i1
Published by the American Institute of Physics.

Optical gain analysis of c-InGaN quantum wells on unstrained c-$In_{0.31}Ga_{0.69}N$ templates

Teruhisa Kotani,[1,2,a)] Paolo Lugli,[1,b)] and Chihiro Hamaguchi[2]
[1]*Institute for Nanoelectronics, Technische Universität München, D-80333 Munich, Germany*
[2]*Advanced Technology Research Laboratories, Sharp Corporation, 2613-1 Ichinomoto-cho, Tenri, Nara 632-8567, Japan*

(Received 18 October 2012; accepted 19 December 2012; published online 10 January 2013)

We investigate the optical properties of c-$In_xGa_{1-x}N$ ($x = 0.31$–0.44) quantum wells (QWs) on unstrained c-$In_{0.31}Ga_{0.69}N$ templates in the green-to-red spectral range using self-consistent multiband k · p theory. The transverse-electric- and transverse-magnetic-polarized optical gains are much higher for QWs on unstrained c-$In_{0.31}Ga_{0.69}N$ templates compared with conventional templates because of a smaller internal electric field and strong valence band mixing. Using c-$In_xGa_{1-x}N$ QWs on c-$In_{0.31}Ga_{0.69}N$ templates is expected to reduce the threshold carrier density in the green range and extend the operable wavelength into the red range. © *2013 American Institute of Physics*. [http://dx.doi.org/10.1063/1.4774290]

InGaN quantum well (QW)-based laser diodes (LDs) on c-GaN templates are highly efficient semiconductor light sources in the short-wavelength visible spectral range. However, the performance of these devices decreases in the blue-green range as the emission wavelength gets longer,[1–3] or in other words, as the indium content in the InGaN QWs increases. Currently, the longest wavelength available using a c-GaN template is limited around 530 nm,[2,4] even though the bandgap of InGaN can be tuned to near-infrared range. This long wavelength limit is mainly due to the large lattice mismatch between the InGaN QWs and the c-GaN template. Strain in InGaN QWs leads to a large piezoelectric polarization in the QWs[5] and phase separation in an InGaN alloy.[6,7] The internal electric field, induced by the different spontaneous and piezoelectric polarizations of the well and barrier materials, separates electrons and holes in the QWs and leads to a reduction in their wave function overlap.[5] Since there is no commercial semiconductor light source in the green-to-red range including the other semiconductor materials, this range is often called the "green gap."

One promising approach to realize the green gap device is to use unstrained c-InGaN templates.[8–11] The theoretical calculation shows the enhancement in the spontaneous emission rate of c-InGaN QWs on c-$In_xGa_{1-x}N$ ($x = 0.05$–0.20) templates in the blue-to-red spectral range.[11]

Recently, unstrained (lattice-matched) c-$In_{0.31}Ga_{0.69}N$ films have been grown on (001)-spinel substrates.[12] Since the bandgap of unstrained c-$In_{0.31}Ga_{0.69}N$ is in the center of the green range (~2.4 eV),[12] c-InGaN QWs on unstrained c-$In_{0.31}Ga_{0.69}N$ templates would have a smaller lattice mismatch than those on conventional c-GaN templates, which would improve LDs performance in the green spectral range. However, neither theoretical nor experimental optical properties of $In_xGa_{1-x}N$ QWs on c-$In_{0.31}Ga_{0.69}$ templates have been reported because studies based on unstrained c-$In_{0.31}Ga_{0.69}$ templates are still in an early stage of development.

In this letter, we calculate the electronic band structure of c-$In_xGa_{1-x}N$ and the optical gain properties of c-$In_xGa_{1-x}N$ ($x = 0.31$–0.44) QWs on unstrained c-$In_{0.31}Ga_{0.69}N$ templates at room temperature. The optical gains are also compared with those on conventional c-GaN templates in the green-to-red spectral range.

The band structure and wave functions are obtained by solving the 1-band effective mass equation for electrons and the 6-band k · p Hamiltonian for holes.[13–15] We also take into account the strain effect, spontaneous and piezoelectric polarization, and self-consistent screening effect.[14] The quasi-Fermi levels are determined self-consistently from the integration of the two-dimensional density of states in the QWs and using the charge neutrality condition when the electron and hole density are both the same as the injected carrier density (n_{2D}). To account for the broadening effect, we use the sech function[16] with a homogeneous broadening of 25 meV.[16] We do not consider the inhomogeneous broadening caused by indium fluctuations in the QWs,[16,17] because no experimental data are available for c-$In_xGa_{1-x}N$ QWs on c-$In_{0.31}Ga_{0.69}N$ templates. We believe that c-$In_xGa_{1-x}N$ ($x = 0.31$–0.44) QWs on unstrained c-$In_{0.31}Ga_{0.69}N$ templates would have smaller (or at least equivalent) indium fluctuations[12] than those on conventional c-GaN templates, if growth conditions are optimized in the future, because of the smaller lattice mismatch between the QWs and the templates. All the material parameters for the InGaN alloys used here are obtained from Refs. 18–20. The optical gains are calculated for two-dimensional carrier densities (n_{2D}) of 6.3×10^{11} to 1.2×10^{13} cm^{-2}.

We consider a QW consisting of 3 nm of c-$In_xGa_{1-x}N$ sandwiched by two 6 nm barrier consisting of c-$In_yGa_{1-y}N$ on c-$In_{0.31}Ga_{0.69}N$ or c-GaN templates for all structures.

Table I shows the indium compositions of the c-$In_xGa_{1_x}N$ (well)/$In_yGa_{1-y}N$ (barrier) QWs and the internal electric fields (F [MV/cm]) of the wells. The indium compositions in the wells are adjusted so that the peak wavelength range corresponds to 525, 550, 575, or 600 nm at an operating carrier density of $n_{2D} = 1.1 \times 10^{13}$ cm^{-2}. We carefully select the well and barrier parameters so that those would be

a)Electronic mail: kotani.teruhisa@sharp.co.jp.
b)Electronic mail: lugli@nano.ei.tum.de.

TABLE I. Indium composition of c-$In_xGa_{1-x}N$ (well)/$In_yGa_{1-y}N$ (barrier) QWs and the internal electric fields (F) in the c-$In_xGa_{1-x}N$ well. The peak wavelengths (WLs) correspond to those for $n_{2D} = 1.1 \times 10^{13}$ cm^{-2}.

	QWs on $In_{0.31}Ga_{0.69}N$			QWs on GaN		
WL range (nm)	x	y	F (MV/cm)	x	y	F (MV/cm)
525	0.31	0.20	1.10	0.32	0	3.63
550	0.35	0.25	1.07	0.34	0	3.90
575	0.40	0.30	1.13	0.37	0	4.30
600	0.44	0.31	1.50	0.40	0	4.69

capable of being grown and be close to the reported green LDs.[2] The 3 nm is near the typical well width of c-$In_xGa_{1_x}N$ QWs for the long wavelength LDs.[2,16] We employ an indium composition smaller by approximately 0.1 in the barrier layers than that in the well on the c-$In_{0.31}Ga_{0.69}N$ templates for efficient carrier confinement and the small lattice mismatch in the 525–575 nm range. Thus, the internal electric fields in the QWs in this range are expected to be similar values. We employ the unstrained barrier layer in the 600 nm range of the c-$In_xGa_{1_x}N$ QWs on the c-$In_{0.31}Ga_{0.69}N$ template and in all spectral ranges of those on GaN templates. Compared with QWs on c-$In_{0.31}Ga_{0.69}N$ templates, those on GaN templates have an internal electric field that is 3–4 times larger. The required indium composition in the QWs for similar wavelengths on both the c-$In_{0.31}Ga_{0.69}N$ and GaN templates is different because of the differences in the band offset and internal electric fields (mainly piezoelectric fields) among the QWs.

Figs. 1(a) and 1(b) show the valence band energies E and effective masses m of the three valence bands (the heavy-hole (HH), light-hole (LH), and crystal-field split-off hole (CFH) bands), respectively, at the $\Gamma(\boldsymbol{k} = 0)$ point of a bulk c-$In_xGa_{1-x}N$ on a $In_{0.31}Ga_{0.69}N$ template as a function of the indium composition x. The LH and CFH bands exhibit an anticrossing interaction and exchange effective mass near $x = 0.29$. The HH and LH bands are almost degenerate ($E_{hh} - E_{lh}$ is less than 10 meV) for $x > 0.31$. However, the separation between the CFH and HH (or LH) bands increases as the indium composition increases ($E_{cfh} - E_{hh}$ is 21.8 meV for $x = 0.31$ and 88 meV for $x = 0.44$). The c-$In_xGa_{1-x}N$ film on an $In_{0.31}Ga_{0.69}N$ template is under tensile strain ($x < 0.31$), lattice matched ($x = 0.31$), or under compressive strain ($x > 0.31$) over the indium composition range. This strain dependent valence band energy and effective mass in the c-$In_xGa_{1-x}N$ film on an $In_{0.31}Ga_{0.69}N$ template are similar to those in c-$In_xGa_{1-x}N$ on c-$In_{0.15}Ga_{0.85}N$ (Ref. 9) and bulk-GaN.[21] The small separation of three valence bands, especially the CFH band near $x = 0.31$, results in complex gain properties.

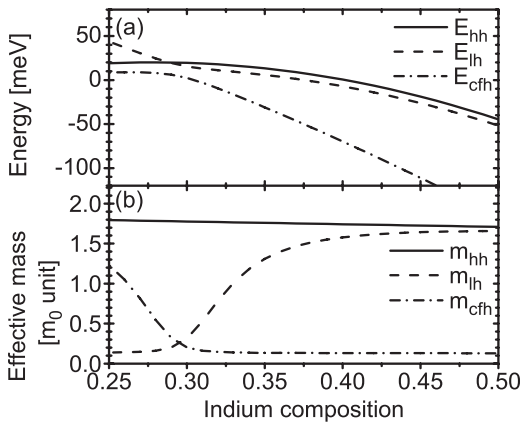

FIG. 1. (a) The energy position of the three valance bands E_{hh}, E_{lh}, and E_{cfh}, and (b) the effective hole masses m_{hh}, m_{lh}, and m_{ch} corresponding to the three valance bands as a function of the indium composition for bulk c-$In_xGa_{1-x}N$ grown on $In_{0.31}Ga_{0.69}N$ templates.

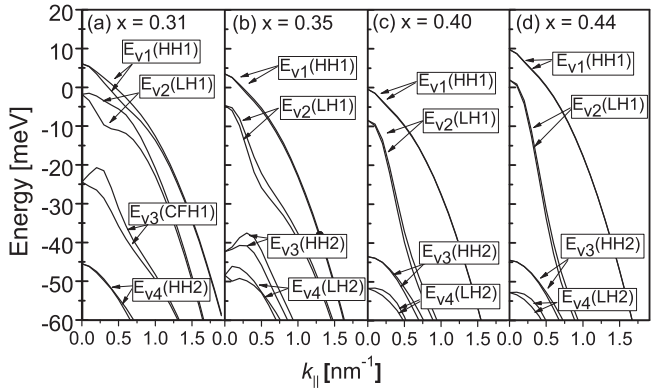

FIG. 2. $E - k_{\|}$ relation and the dominant subband state at the band edge ($k_{\|}$) of the c-$In_xGa_{1-x}N$/$In_yGa_{1-y}N$ QWs on c-$In_{0.31}Ga_{0.69}N$ templates at a carrier density of $n_{2D} = 1.1 \times 10^{13}$ cm^{-2}. The HHi (LHi, CFHi) shows the i-th ($i = 1$ is ground) state of the HH (LH, CFH) subbands. The 0 eV of the vertical axis corresponds to the unstrained and unscreened valence band energy in the well. Only the x values are shown to identify the QW structures.

Figs. 2(a)–2(d) show the valence subband structure along the $k_{\|}$ (in-plane) direction of the c-$In_xGa_{1-x}N$/$In_yGa_{1-y}N$ QWs on c-$In_{0.31}Ga_{0.69}N$ templates at a carrier density of $n_{2D} = 1.1 \times 10^{13}$ cm^{-2}. Since the QWs are not symmetric due to the internal electric field, the subband energies for spin up and spin down are not degenerate; they are only degenerate at $k_{\|} = 0$. Table II shows the hole population ratio in the top four valence subbands (P_{v1} to P_{v4}). As the indium composition increases, the subband energy spacing increases, and this increase reduces the hole population in the higher subbands. The HH, LH, and CFH states are strongly mixed in all subbands, and the mixing rates depend highly on the indium composition and $k_{\|}$. The dominant states in valence bands E_{v1} and E_{v2} are the HH1 and LH1 states, respectively, for all indium compositions at $k_{\|} = 0$. In E_{v3}, the CFH1 state is the dominant state for $x = 0.31$, and the HH2 state is the dominant state for $x = 0.35$, 0.40, and 0.44 at $k_{\|} = 0$. In E_{v4}, the HH2 state is the dominant state for $x = 0.31$, and the LH2 state is the dominant state for

TABLE II. Hole population ratios in each valence subband of c-$In_xGa_{1-x}N$/$In_yGa_{1-y}N$ QWs on c-$In_{0.31}Ga_{0.69}N$ templates. The P_{vi} value represents the hole population ratio for ith-valence subband (E_{vi}). Only x values are shown to identify the QW structures.

x	P_{v1} (%)	P_{v2} (%)	P_{v3} (%)	P_{v4} (%)
0.31	45	31	12	5
0.35	48	24	9	7
0.40	55	17	9	6
0.44	65	16	8	5

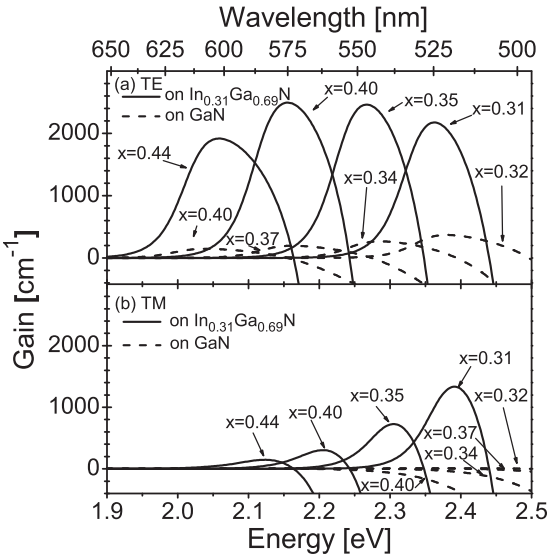

FIG. 3. (a) TE- and (b) TM-polarized gain spectra of c-$In_xGa_{1-x}N$/$In_yGa_{1-y}N$ QWs on c-$In_{0.31}Ga_{0.69}N$ (solid lines) and c-GaN (dashed lines) templates at a carrier density of $n_{2D} = 1.1 \times 10^{13}\,cm^{-2}$. Only the x values are shown to identify the QW structures.

$x = 0.35$, 0.40, and 0.44 at $k_{\|} = 0$. The mixing at $k_{\|} > 0$ is more complex. For example, CFH1 becomes the dominant state at $k_{\|} > 0.2\,nm^{-1}$ of E_{v3} for $x = 0.35$. Mixing of the CFH states changes from the higher energies to lower energies as the indium composition increases because the position of the CFH band edge gets lower as indium composition increases as shown in Fig. 1.

Figs. 3(a) and 3(b) show the transverse-electric (TE)- and transverse-magnetic (TM)-polarized gain spectra, respectively, of the QWs in Table I at $n_{2D} = 1.1 \times 10^{13}cm^{-2}$. Figs. 4(a) and 4(b) show the TE- and TM-polarized maximum gain as a function of n_{2D}, respectively. QWs on c-$In_{0.31}Ga_{0.69}N$ templates have higher maximum gains and gain slopes than those on c-GaN templates for all indium compositions and both polarizations. For example, at $n_{2D} > 7 \times 10^{12}\,cm^{-2}$, QWs on c-$In_{0.31}Ga_{0.69}N$ templates have a TE-polarized gain that is 5–6 times higher in the 525 nm range, 7–8 times higher in the 550 nm range, and 10–12 times higher in the 575 and 600 nm ranges than that on c-GaN templates. This is mainly due to the internal electric fields in the QWs on the c-$In_{0.31}Ga_{0.69}N$ template being smaller by a factor of 1/4–1/3. As x increases, the maximum TE-polarized gain decreases in the QWs on the c-GaN templates because the internal electric fields in the QWs also increase as shown in Table I. The maximum TE-polarized gain of the QWs on c-$In_{0.31}Ga_{0.69}N$ templates increases for $x = 0.31$–0.35, does not change at $x = 0.35$ or 0.40, and decreases for $x = 0.40$–0.44. In contrast, the maximum TM-polarized gain of the QWs on c-$In_{0.31}Ga_{0.69}N$ templates decreases as x increases, whereas the QWs on c-GaN templates, it is less than $10\,cm^{-1}$ at $n_{2D} = 1.1 \times 10^{13}\,cm^{-2}$ for all x. The gain behavior of the QWs on c-$In_{0.31}Ga_{0.69}N$ templates is due to a combination of band mixing and the internal electric fields.

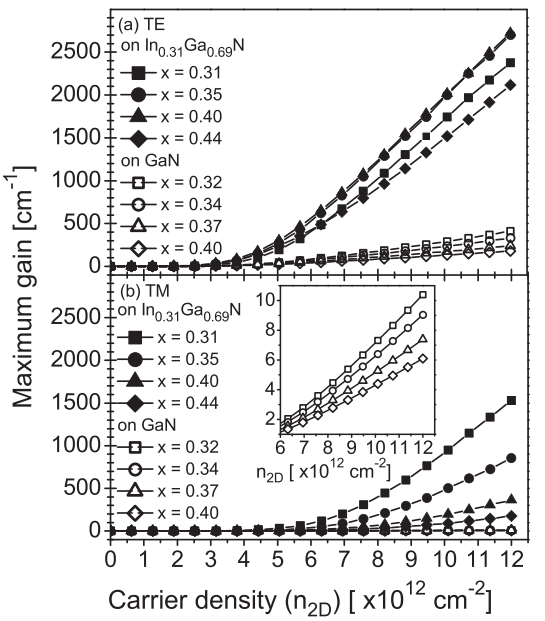

FIG. 4. Maximum (a) TE- and (b) TM-polarized gains of c-$In_xGa_{1-x}N$/$In_yGa_{1-y}N$ QWs on c-$In_{0.31}Ga_{0.69}N$ (solid symbols) and c-GaN (open symbols) templates as a function of the carrier density. Only the x values are shown to identify the QW structures. The inset in (b) shows details of the maximum gain of the c-$In_xGa_{1-x}N$ QWs on c-GaN templates.

Table III shows the decomposed TE- and TM-polarized gains generated from the transition between the first conduction subband (E_{c1}) and the first to fourth valence subbands (E_{v1} to E_{v4}) at $n_{2D} = 1.1 \times 10^{13}\,cm^{-2}$. The TE-polarized gains (g_{ij}^{TE}) are mainly generated from the E_{c1} to E_{v1} transition, while the TM-polarized gains (g_{ij}^{TM}) are mainly generated from the E_{c1} to E_{v3} transition for $x = 0.31$ and 0.35, and the E_{c1} to E_{v4} transition for $x = 0.40$ and 0.44. In other words, a transition that generates a TM-polarized gain shifts from a lower to higher valence subband as the indium composition increases. In wurtzite crystals, the transitions between the conduction and HH or LH states contribute to the TE-polarized gain, and the transition between the conduction and CFH states contribute to the TM-polarized gain.[14] As shown in Fig. 1(a), the CFH band is located near the HH and LH bands at $x \sim 0.31$ and it shifts to a lower energy as the indium composition increases. Therefore, mixing of the CFH state in the QWs also shifts from lower to higher subbands. Moreover, as shown in Table II, higher valence subbands have a lower hole population ratio than the lower valence subbands, and

TABLE III. The decomposed gains at the TE(TM-) gain peak energies of c-$In_xGa_{1-x}N$/$In_yGa_{1-y}N$ QWs on c-$In_{0.31}Ga_{0.69}N$ templates. The $g_{ij}^{TE(TM)}$ value represents TE(TM)-polarized gain between the ith-conduction subband (E_{ci}) and the jth-valence subband (E_{vj}).

	TE-polarized gains			
x	g_{11}^{TE} (cm^{-1})	g_{12}^{TE} (cm^{-1})	g_{13}^{TE} (cm^{-1})	g_{14}^{TE} (cm^{-1})
0.31	1524	665	10	35
0.35	1751	683	35	39
0.40	1784	622	66	38
0.44	1376	478	35	19
	TM-polarized gains			
x	g_{11}^{TM} (cm^{-1})	g_{12}^{TM} (cm^{-1})	g_{13}^{TM} (cm^{-1})	g_{14}^{TM} (cm^{-1})
0.31	75	418	1029	15
0.35	26	92	568	39
0.40	11	15	102	135
0.44	6	8	44	74

the TM-polarized gain generated by the transition between the conduction and CFH state is much smaller for high x values. Less CFH band mixing in the lower valence subband means fewer holes contribute to the TM-polarized gain and more holes contribute to the TE-polarized gain, as evidenced by the TM-polarized gain reduction for $x = 0.31$–0.44 and the TE-polarized gain increase for $x = 0.31$–0.40. As shown in Table I, the internal electric field of the c-$In_xGa_{1-x}N$ QWs on c-$In_{0.31}Ga_{0.69}N$ templates for $x = 0.44$ is 1.3 to 1.4 times stronger than those for $x = 0.31$–0.40. This results in a decrease in the TE-polarized gain for $x = 0.40$–0.44.

If a confinement factor (Γ) of 0.016,[16] an internal loss (α_i) of $8\,cm^{-1}$,[4] and a mirror loss (α_m) of $6.3\,cm^{-1}$ (for a cavity length of 1 mm and mirror reflectivities of 0.95 and 0.30) for TE-polarized light in the green spectral range are assumed, the threshold gain is $\alpha_i/\Gamma = 893\,cm^{-1}$. Therefore, c-$In_xGa_{1-x}N$ ($x = 0.31$–0.44) QWs on c-$In_{0.31}Ga_{0.69}N$ templates start TE-polarized lasing for a carrier density of $n_{2D} = 7 - 8 \times 10^{12}\,cm^{-2}$. In contrast, c-$In_xGa_{1-x}N$ ($x = 0.33$–0.40) QWs on c-GaN templates need a carrier density higher than $n_{2D} = 1.2 \times 10^{13}\,cm^{-2}$ to achieve lasing. In addition, the high TM-polarized gain of the c-$In_xGa_{1-x}N$ QWs on c-$In_{0.31}Ga_{0.69}N$ templates suggests the possibility of the TM-polarized lasing if one properly tunes the QW parameters and the cavity structures so that the TM-polarized modal gain is higher than or comparable to the TE-polarized modal gain.

In summary, we investigate the electronic and gain properties of c-$In_xGa_{1-x}N$ QWs on c-$In_{0.31}Ga_{0.69}N$ templates in the green-to-red spectral range. We have found that c-InGaN QWs on c-$In_{0.31}Ga_{0.69}N$ template have the 5–12 times higher TE-polarized gain than these on c-GaN template in 525–600 nm range. We have also found that the strong CFH state mixing contributes the TM-polarized gain for $x \sim 0.31$. As x increases, the CFH state mixing moves to lower energy and the TM-polarized gain decreases. Our result demonstrates that c-InGaN QWs on c-$In_{0.31}Ga_{0.69}N$ templates should be able to improve the performance in green nitride LDs and extend the operatable spectral range of nitride LDs into the red range.

The authors would like to acknowledge K. Ohta, A. Takahashi, and Y. Murakami in Sharp Corporation for their encouragement and support for this work.

[1]T. Miyoshi, S. Masui, T. Okada, T. Yanamoto, T. Kozaki, S. Nagahama, and T. Mukai, Appl. Phys. Express **2**, 062201 (2009).
[2]A. Avramescu, T. Lermer, J. Müller, C. Eichler, G. Bruederl, M. Sabathil, S. Lutgen, and U. Strauss, Appl. Phys. Express **3**, 061003 (2010).
[3]A. Avramescu, T. Lermer, J. Müller, S. Taulz, D. Queren, S. Lutgen, and U. Strauss, Appl. Phys. Lett. **95**, 071103 (2009).
[4]J. Müller, U. Strauss, T. Lermer, G. Bruderl, C. Eichler, and A. Avramescu, Phys. Status Solidi A **208**, 1590 (2011).
[5]V. Fiorentini, F. Bernardini, F. D. Sala, A. D. Carlo, and P. Lugli, Phys. Rev. B **60**, 8849 (1999).
[6]I. H. Ho and G. B. Stringfellow, Appl. Phys. Lett. **69**, 2701 (1996).
[7]R. Singh, D. Doppalapudi, T. D. Moustakas, and L. T. Romano, Appl. Phys. Lett. **70**, 1089 (1997).
[8]T. K. Sharma and E. Towe, J. Appl. Phys. **106**, 104509 (2009).
[9]T. K. Sharma and E. Towe, J. Appl. Phys. **107**, 024516 (2010).
[10]T. K. Sharma and E. Towe, Appl. Phys. Lett. **96**, 191105 (2010).
[11]J. Zhang and N. Tansu, J. Appl. Phys. **110**, 113110 (2011).
[12]A. G. Norman, P. C. Dippo, H. R. Moutinho, J. Simon, and A. J. Ptak, Appl. Phys. Lett. **100**, 152106 (2012).
[13]C. Hamaguchi, *Basic Semiconductor Physics*, 2nd ed. (Springer-Verlag, 2010), Chap. 9, pp. 443–510.
[14]S. L. Chuang, IEEE J. Quantum Electron. **32**, 1791 (1996).
[15]S. L. Chuang and C. S. Chang, Semicond. Sci. Technol. **12**, 252 (1997).
[16]U. T. Schwarz, H. Braun, K. Kojima, M. Funato, Y. Kawakami, S. Nagahama, and T. Mukai, Proc. SPIE **6485**, 648506 (2007).
[17]K. Kojima, U. T. Schwarz, M. Funato, Y. Kawakami, S. Nagahama, and T. Mukai, Opt. Express **15**, 7730 (2007).
[18]I. Vurgaftman and J. R. Meyer, J. Appl. Phys. **94**, 3675 (2003).
[19]I. Vurgaftman and J. Meyer, *Nitride Semiconductor Devices* (Wiley, 2007), Chap. 2, pp. 13–48.
[20]M. Ueda, M. Funato, K. Kojima, Y. Kawakami, Y. Narukawa, and T. Mukai, Phys. Rev. B **78**, 233303 (2008).
[21]A. Shikanai, T. Azuhata, T. Sota, S. Chichibu, A. Kuramata, K. Horino, and S. Nakamura, J. Appl. Phys. **81**, 417 (1997).